Sciences & Technologie **A** – **N°22**, Décembre (2004), pp. 39-52.

THE PHYSICAL ASPECT OF THREE-DIMENSIONAL MIXED CONVECTION IN A UNIFORMLY HEATED HORIZONTAL PIPE

Received 07/07/2004 – Accepted 31/12/2004

Abstract

This study concerns the numerical simulation of the three dimensional forced and mixed convection heat transfer in a uniformly horizontal heated pipe. The complete Navier-Stokes equations are numerically solved with a finite volume method.. The obtained results show that the mixed convection flow is quite three-dimensional. As the Grashof number is increased, a secondary flow develops in the form of a two counter-rotating vortices. The vortices lead to a better mixing of the flow and thus enhance the convective heat transfer: the local axial Nu decreases along an entrance region and then increases downstream instead of leveling off as in the case of forced convection. The increase is more important for higher Richardson numbers.

***Keywords**: horizontal pipe / uniform heating / laminar mixed convection / numerical simulation.*

Résumé

Cette étude concerne une simulation numérique tridimensionnelle d'un transfert thermique en convection forcée et en convection mixte dans un conduit horizontal uniformément chauffé. Les équations complètes de Navier-Stokes sont numériquement résolues par la méthode des volumes finis. Les résultats obtenus montrent que l'écoulement est tridimensionnel. Au fur et à mesure que le nombre de Grashof augmente, un écoulement secondaire se développe sous la forme de deux vortex contrarotatifs. Ces vortex conduisent à un meilleur brassage de l'écoulement et de ce fait augmente le transfert thermique convectif: le nombre de Nu local axial diminue le long de la zone d'entrée puis, à l'aval du conduit, il subit une croissance en se détachant du Nu correspondant à celui de la convection forcée. Cette croissance est d'autant plus importante pour des nombres de Richardson élevés.

***Mots clés**: conduit horizontal / chauffage uniforme / convection mixte laminaire / simulation numérique.*

T. BOUFENDI
M. AFRID
Lab. de Physique Energétique
Département de Physique
Faculté des Sciences
Université Mentouri
Constantine (Algérie)

ملخص

هذه الدراسة تهتم بالتشابه العددي الثلاثي الأبعاد للتحويل الحراري بالحمل الإجباري والمختلط داخل أنبوب أفقي ذات تسخين متجانس. تحل معادلات Navier-Stokes الإجمالية عدديا باستعمال طريقة الأحجام المنتهية. أثبتت النتائج المحصل عليها بأن الجريان هو ثلاثي الأبعاد. يؤدي الازدياد في عدد Grashof إلى نمو جريان ثانوي يكون على شكل دوامتين متعاكستي الدوران. قد تعطي الدوامات أحسن امتزاج للجريان حيث يؤدي إلى ازدياد التبادل الحراري بالحمل: إن عدد Nu المحلي المحوري يتناقص عبر منطقة المدخل، ثم يزداد في منطقة المخرج المتبقية مع ابتعاده من Nu الموافق للحمل المجبر. هذا الازدياد يوافق الازدياد في عدد Richardson.

***الكلمات المفتاحية:** أنبوب أفقي/ التسخين المتجانس/ حمل مختلط/ تشابه عددي.*

Fundamental research in convective heat transfer in cylindrical pipes has gained a lot of consideration in the thermal science literature because of its numerous industrial applications. Important applications include heat exchangers, combustion systems and solar plants to name just a few.

Mixed convection studies have been reported since the sixties. The studies of Mori *et al.* [1], Shannon and Depew [2,3], Hussaïn and McComas [4] and Petukhov and Polyakov [5] have revealed the experimental evidence of the contribution of buoyancy forces to the considered laminar forced convective heat transfer between horizontal heated pipes and flows of air, water and ethylene glycol. These studies reported mixed convection average Nusselt numbers that are 2.5 times those of forced convection. Bergles and Simonds [6] have studied experimentally the mixed convective heat transfer between a heated glass pipe and a laminar flow of water for Reynolds numbers in the range 460-800 and Rayleigh numbers in the range 10^4-10^6 . They found that the mixed convection Nusselt number is three to four times that of the forced convection. Similar results are reported by Hong *et al.* [7] and Morcos and Bergles [8]. Recently Abid *et al.* [9] have studied the mixed convection in a uniformly heated pipe of finite thickness transporting water. The heating is produced with Joulean effect in the entire wall thickness of the tube. They used Infra-Red Imaging to determine the axially increasing wall pipe temperature.

There has been many numerical studies concerning the problem of mixed convection in a uniformly heated horizontal pipe. As examples, we cite the work of Newell and Bergles [10] using a finite differences method and have presented the stable thermal stratification and reported a significant Nusselt number increase. The case of a non uniformly heated horizontal pipe transporting air has been numerically studied by Patankar

et al. [11]. The two-dimensional radial-angular flow mathematical model is numerically solved by the finite volume method. The Gr^* is varied from 10 to 10^7. The flow field is represented by four counter-rotating cells at higher Gr^*. The same problem is considered by Law *et al.* [12]. For Gr^* of the order of 10^5, the results are comparable to those of [11]; however, for higher Gr^*, the flow is represented by two counter-rotating cells instead of four. In our study, we will demonstrate that for the considered range of Ri, the secondary flow is represented by two counter-rotating cells. The simultaneously developing mixed convection in an inclined heated pipe is considered in the recent numerical study of Ouzzane and Galanis [13]. Four different cases have been simulated: the pipe thickness is considered or neglected and in each case the heating is over the entire circumference or over the top half of it, the lower half being insulated.

In our present study, we consider the numerical simulation of the three-dimensional forced and mixed convection in a uniformly heated horizontal pipe. The main objective of our study is the illustration and the explanation of the physical differences between the forced and the mixed convection and the effect at higher Richardson numbers

1- THE GEOMETRY AND THE MATHEMATICAL MODEL

Figure 1 illustrates the geometry and the considered hydrodynamic and thermal boundary conditions. A long horizontal pipe having an aspect ratio A=100 is uniformly heated by a constant heat flux and is used to heat a laminar incompressible flow of a Newtonian fluid (water). At the pipe entrance the flow is considered a Poiseuille flow having a parabolic radial profile. At the pipe exit, the convective fluxes of momentum are considered much greater than the diffusive ones justifying the use of null velocity gradients at the pipe exit. At the same location, the axial heat flux is assumed constant, justifying the use of a null second derivative of the temperature. The fluid physical properties (except the density) are assumed constants (evaluated at an appropriate temperature). The density is a linear function of temperature and the Boussinesq approximation is applied.

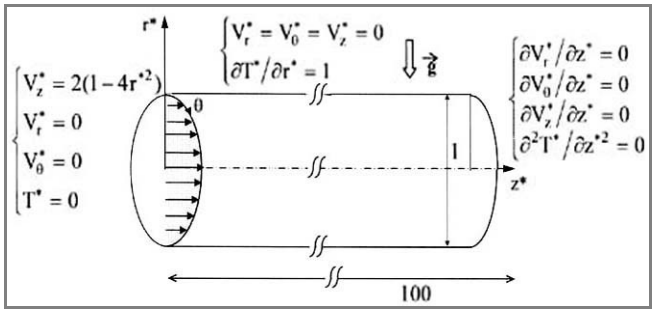

Figure 1: Geometry and boundary conditions.

The physical principles involved in this problem are the conservation of mass, momenta and energy. They are well modeled by the following system of conservation partial differential equations:

The initial conditions:

At $t^* = 0$ for $0 \le r^* \le 0.5$, $0 \le \theta \le 2\pi$ and $0 \le z^* \le 100$:

$$V_r^* = V_\theta^* = V_z^* = T^* = 0$$

For times $t^* > 0$:

Mass conservation equation:

$$\frac{1}{r^*}\frac{\partial}{\partial r^*}\left(r^* V_r^*\right) + \frac{1}{r^*}\frac{\partial V_\theta^*}{\partial \theta} + \frac{\partial V_z^*}{\partial z^*} = 0 \qquad (1)$$

Radial momentum conservation equation:

$$\frac{\partial V_r^*}{\partial t^*} + \left(\frac{1}{r^*}\frac{\partial}{\partial r^*}(r^* V_r^* V_r^*) + \frac{1}{r^*}\frac{\partial}{\partial \theta}(V_\theta^* V_r^*) - \frac{V_\theta^{*2}}{r^*} + \frac{\partial}{\partial z^*}(V_z^* V_r^*)\right) =$$

$$-\frac{\partial P^*}{\partial r^*} + \frac{\mathbf{Gr}^*}{\mathbf{Re}^2}\cos\theta\ T^*$$

$$+\frac{\mathbf{1}}{\mathbf{Re}}\left[\frac{\partial}{\partial r^*}\left(\frac{1}{r^*}\frac{\partial}{\partial r^*}(r^* V_r^*)\right) + \frac{1}{r^{*2}}\frac{\partial}{\partial \theta}\left(\frac{\partial V_r^*}{\partial \theta}\right)\right.$$

$$\left. -\frac{2}{r^{*2}}\frac{\partial V_\theta^*}{\partial \theta} + \frac{\partial}{\partial z^*}\left(\frac{\partial V_r^*}{\partial z^*}\right)\right] \qquad (2)$$

Angular momentum conservation equation:

$$\frac{\partial V_\theta^*}{\partial t^*} + \left(\frac{1}{r^*}\frac{\partial}{\partial r^*}(r^* V_r^* V_\theta^*) + \frac{1}{r^*}\frac{\partial}{\partial \theta}(V_\theta^* V_\theta^*) + \frac{V_r^* V_\theta^*}{r^*} + \frac{\partial}{\partial z^*}(V_z^* V_\theta^*)\right) =$$

$$-\frac{1}{r^*}\frac{\partial P^*}{\partial \theta} - \frac{\mathbf{Gr}^*}{\mathbf{Re}^2}\sin\theta\ T^*$$

$$+\frac{\mathbf{1}}{\mathbf{Re}}\left[\frac{\partial}{\partial r^*}\left(\frac{1}{r^*}\frac{\partial}{\partial r^*}(r^* V_\theta^*)\right) + \frac{1}{r^{*2}}\frac{\partial}{\partial \theta}\left(\frac{\partial V_\theta^*}{\partial \theta}\right)\right.$$

$$\left. +\frac{2}{r^{*2}}\frac{\partial V_r^*}{\partial \theta} + \frac{\partial}{\partial z^*}\left(\frac{\partial V_\theta^*}{\partial z^*}\right)\right] \qquad (3)$$

Axial momentum conservation equation:

$$\frac{\partial V_z^*}{\partial t^*} + \left(\frac{1}{r^*}\frac{\partial}{\partial r^*}(r^* V_r^* V_z^*) + \frac{1}{r^*}\frac{\partial}{\partial \theta}(V_\theta^* V_z^*) + \frac{\partial}{\partial z^*}(V_z^* V_z^*)\right) =$$

$$-\frac{\partial P^*}{\partial z^*} + \frac{\mathbf{1}}{\mathbf{Re}}\left[\left(\frac{1}{r^*}\frac{\partial}{\partial r^*}\left(r^*\frac{\partial V_z^*}{\partial r^*}\right)\right)\right.$$

$$\left. +\frac{1}{r^{*2}}\frac{\partial}{\partial \theta}\left(\frac{\partial V_z^*}{\partial \theta}\right) + \frac{\partial}{\partial z^*}\left(\frac{\partial V_z^*}{\partial z^*}\right)\right] \qquad (4)$$

Energy conservation equation :

$$\frac{\partial T^*}{\partial t^*} + \left(\frac{1}{r^*}\frac{\partial}{\partial r^*}(r^* V_r^* T^*) + \frac{1}{r^*}\frac{\partial}{\partial \theta}(V_\theta^* T^*) + \frac{\partial}{\partial z^*}(V_z^* T^*)\right) =$$

$$\frac{\mathbf{1}}{\mathbf{Re}\,\mathbf{Pr}}\left[\left(\frac{1}{r^*}\frac{\partial}{\partial r^*}\left(r^*\frac{\partial T^*}{\partial r^*}\right)\right) + \frac{1}{r^{*2}}\frac{\partial}{\partial \theta}\left(\frac{\partial T^*}{\partial \theta}\right) + \frac{\partial}{\partial z^*}\left(\frac{\partial T^*}{\partial z^*}\right)\right] \qquad (5)$$

These equations are solved with the following boundary conditions:

At the pipe entrance: $z^* = 0$

for $0 \le r^* \le 0.5$ and $0 \le \theta \le 2\pi$

$$V_r^* = V_\theta^* = T^* = 0 \quad , \quad V_z^* = 2\left(1 - 4r^{*2}\right) \tag{6}$$

At the pipe exit : $z^* = 100$

for $0 \le r^* \le 0.5$ and $0 \le \theta \le 2\pi$

$$\frac{\partial V_r^*}{\partial z^*} = \frac{\partial V_\theta^*}{\partial z^*} = \frac{\partial V_z^*}{\partial z^*} = \frac{\partial^2 T^*}{\partial z^{*2}} = 0 \tag{7}$$

On the pipe axis, the dynamical axial conditions are considered. The computed variables are conveniently interpolated at $r^* = 0$.

At the pipe wall: $r^* = 0.5$

for $0 \le \theta \le 2\pi$ and $0 \le z^* \le 100$

$$V_r^* = V_\theta^* = V_z^* = 0 \quad \text{and} \quad \frac{\partial T^*}{\partial r^*} = 1 \tag{8}$$

Along the angular direction the periodic conditions are imposed:

for $0 \le r^* \le 0.5$ and $0 \le z^* \le 100$

$$\begin{cases} V_r^*(r^*,\ 0\ ,\ z^*, t^*) = V_r^*(r^*,\ 2\pi\ ,\ z^*, t^*) \\ V_\theta^*(r^*,\ 0\ ,\ z^*, t^*) = V_\theta^*(r^*,\ 2\pi\ ,\ z^*, t^*) \\ V_z^*(r^*,\ 0\ ,\ z^*, t^*) = V_z^*(r^*,\ 2\pi\ ,\ z^*, t^*) \\ T(r^*,\ 0\ ,\ z^*, t^*) = T(r^*,\ 2\pi\ ,\ z^*, t^*) \end{cases} \tag{9}$$

At steady state, a simple energy balance on a small portion of the pipe can demonstrate that the local Nusselt number depending on θ and z^* is defined by:

$$Nu(\theta, z^*) = \frac{h(\theta, z^*)\ D}{k} = \frac{1}{\left[T^*(1/2, \theta, z^*) - T_b^*(z^*)\right]} \tag{10}$$

The bulk (mixing cup) non dimensional temperature is defined by:

$$T_b^*(z^*) = \frac{\int_0^{1/2}\int_0^{2\pi} V^*(r^*, \theta, z^*)\, T^*(r^*, \theta, z^*)\, r^*\, dr^*\, d\theta}{\int_0^{1/2}\int_0^{2\pi} V(r^*, \theta, z^*)\, r^*\, dr^*\, d\theta} \tag{11}$$

Another local Nusselt number depending only on the axial coordinate z^* but averaged over the angular coordinate θ can be defined as:

$$Nu(z^*) = \frac{1}{2\pi}\int_0^{2\pi} Nu(\theta, z^*)\, d\theta \tag{12}$$

2- THE NUMERICAL PROCEDURE

The model equations Eqs.(1)-(5) are descretized using the finite volume method, well described by Patankar [14]. The power-law discretization scheme is used in our study. The SIMPLER algorithm [14] is used to obtain the sequential solution of the descretized model equations. The line by line sweeping method, involving the use of the tri-diagonal and the tri-diagonal cyclic matrices solver, is used for the iterative solution of the systems of the descretized equations.

In the r^*, θ, z^* directions, three numerical grids: 22x22x42, 43x44x83 and 43x44x165, were tested to estimate the effect of the grid resolution on the results. It is found that the last two grids give similar results. For example, the figure 2 show this mesh size independence for the fluid temperature at the axis of the tube. The results that will be presented later are those of the 43x44x165 grid. Time marching, with the time step $\Delta t^* = 10^{-3}$, is continued until the steady state is reached. The steady state is checked by the satisfaction of the global mass and energy balances as well as the leveling off of the time evolution of the hydrodynamic and thermal fields.

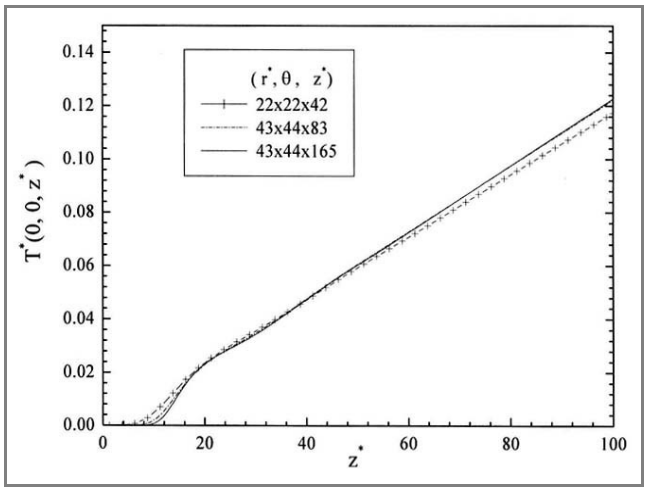

Figure 2: Mesh size influence on the axial evolution of the fluid temperature at the center of the pipe.

The accuracy of the results of our numerical code has been tested by the comparison of our results with previously published results. For the pure forced convection case with a hydrodynamically developed flow, figure 3a shows that the axial evolution of the circumferentially averaged Nusselt number agrees very well with the empirical solution:

$$Nu = 4.36 \ + \ 1.31\ (z^+)^{1/3}\ \exp(-13\ (z^+)^{1/2})$$

where $z^+ = z^* / \mathrm{Re}\,\mathrm{Pr}$, cited in Polyakov [15].

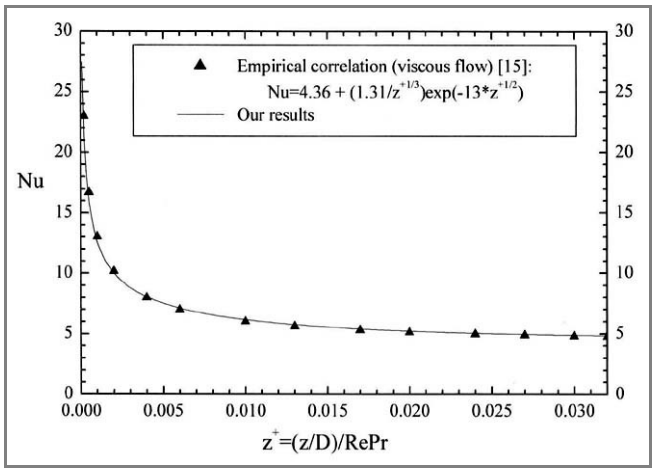

Figure 3a: Validation of the calculated average Nusselt number (forced convection, $Gr^*=0$).

Furthermore, in the mixed convection regime, the figure 3b compare the angular variation of the wall temperature at three axial positions with the results of Ouzzane and Galanis [13]. Their results concern the simultaneously developing heat transfer and fluid flow in a uniformly heated inclined pipe ($\alpha = 40^\circ$). The controlling parameters of the problem are: Re=500, Pr=7.0, Gr=10^6, $L/D = 90$, $R/D = 0.5$. The used grid is 40x36x182 in the r^* , θ , z^* directions, respectively. It is seen that there is a good agreement between our results and theirs.

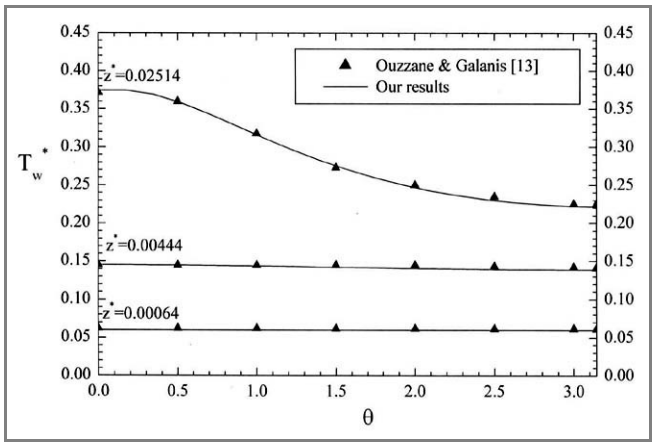

Figure 3b: Comparison of the calculated angular variation of the wall temperature at three axial positions with the results of Ouzzane and Galanis [13].

3- RESULTS

The Reynolds number, the Prandtl number and the Aspect ratio are fixed : $\mathrm{Re} = 1000$, $\mathrm{Pr} = 3.02$ and A=100. However, the Grashof number is varied: three numbers are considered $Gr^* = 0$, $Gr^* = 10^6$ and $Gr^* = 10^7$. The first one, $Gr^* = 0$, corresponds to the forced convection case which is considered our reference state. The latter two numbers, $Gr^* = 10^6$ and $Gr^* = 10^7$, are those of the mixed convection cases with the Richardson number ($Ri = Gr^* / Re^2$) equal to 1 and 10, respectively. These cases represent the effect of the increased intensity of the natural convection and will be compared with the reference state. The flow and thermal fields of each case will be discussed and the heat transfer rates (of the three cases) measured by the values of the local Nusselt numbers will be compared.

3.1- The forced convection reference state ($Gr^* = 0$)

3.1.1- The flow field

The flow and thermal fields of such a case have to be axisymmetric. The imposed pipe entrance flow is of Poiseuille's type: it has only one velocity component, along the axial direction, that is equal to that of the hydrodynamically developed flow. The null radial and angular velocity components at the pipe entrance, the non slip conditions at the pipe wall and the null Gr^* will keep these components equal to zero throughout the pipe. Nothing will induce a change of such values. Thus, the flow will keep its entrance profile throughout the pipe. The axial velocity profile at any pipe section from $z^* = 0$ to $z^* = 100$ is illustrated in figure 4. It is clear that the axial flow is axisymmetric with a parabolic radial profile. The axial velocity increases from zero at the wall to its maximum value (**2**) at the pipe center.

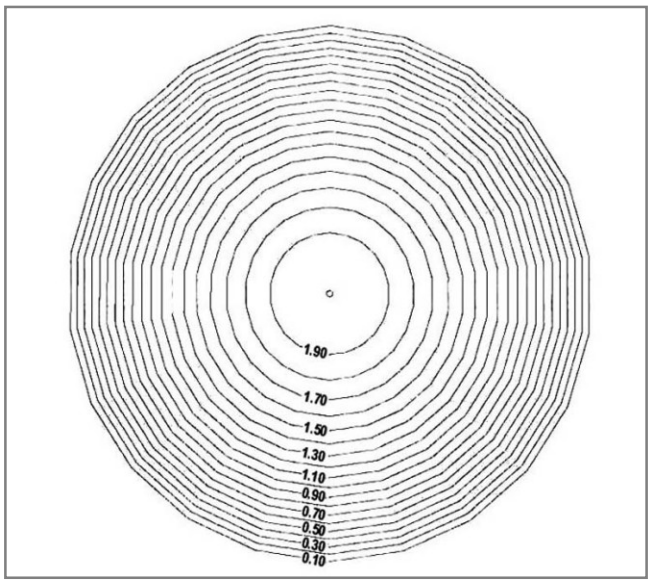

Figure 4: Axial velocity profile at any pipe section for the reference state (Gr^*=0).

3.1.2- The thermal field

The flow enters the pipe at a zero temperature and is heated by a uniformly axisymmetric heat flux at the pipe wall. It is a case of a hydrodynamically developed, thermally developing flow. It is expected that the flow temperature will increase along the axial direction but will be axisymmetric at any pipe section. This is imposed by the null radial and angular velocity components as well as the axisymmetric axial flow and the thermal boundary conditions.

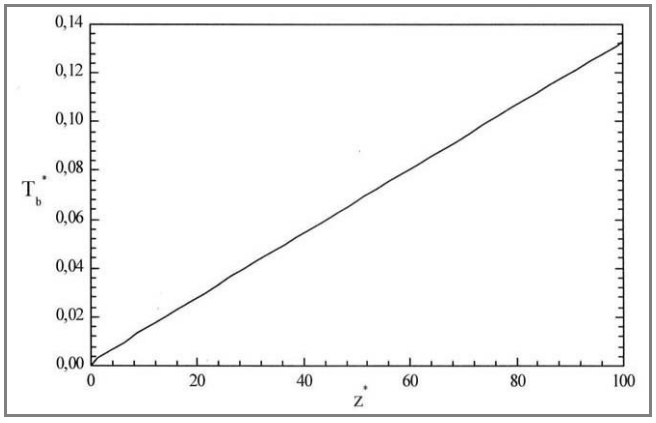

Figure 5: The bulk fluid temperature along the pipe for the reference state.

The mixing cup bulk temperature (as defined in the mathematical model) increases linearly from the entrance to the exit of the pipe as shown in figure 5. This is explained

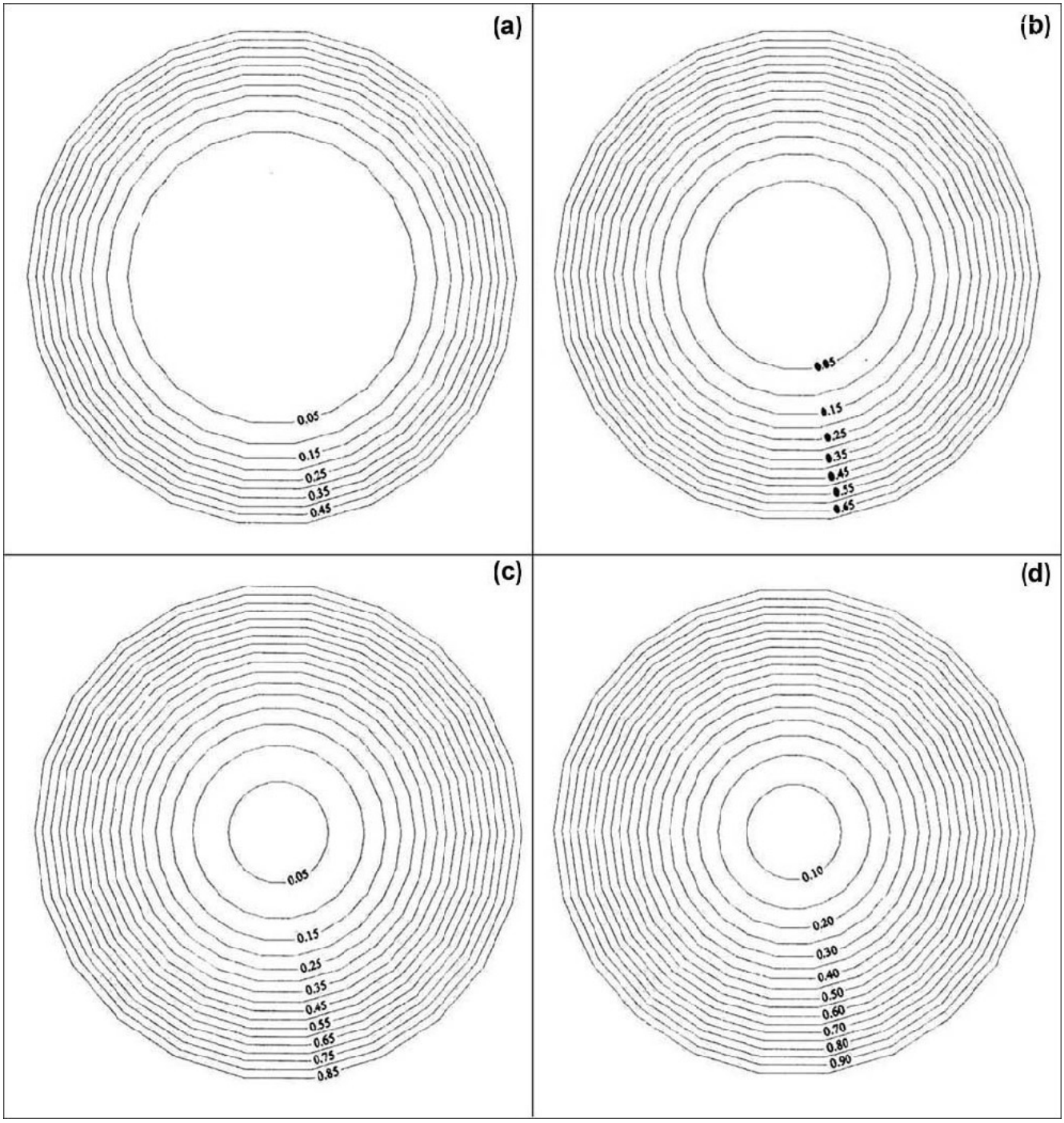

Figure 6: **(a)** Normalized isotherms T^* / T^*_{max} at z*=25 for Gr*=0 ($T^*_{max} = 0.3417$ at the pipe exit).

(b) Normalized isotherms T^* / T^*_{max} at z*=50 for Gr*=0 ($T^*_{max} = 0.3417$ at the pipe exit).

(c) Normalized isotherms T^* / T^*_{max} at z*=75 for Gr*=0 ($T^*_{max} = 0.3417$ at the pipe exit).

(d) Normalized isotherms T^* / T^*_{max} at z*=100 for Gr*=0 ($T^*_{max} = 0.3417$ at the pipe exit).

by the continuous addition of heat as the fluid flows through the pipe. This heat diffuses radially and alters the radial distribution of the temperature. The variation is demonstrated by the graphical presentation of the thermal field at four arbitrarily selected axial stations: $z^* = 25$, $z^* = 50$, $z^* = 75$ and $z^* = 100$. The thermal fields of the selected sections are presented in figures 6a-6d. At each section the non dimensional temperature is normalized by the maximum non dimensional temperature located at the exit of the pipe $(T^* = 0.3417)$. A comparison of the four distributions reveals the increase of the maximum sectional temperature and the increase of heat diffusion towards the pipe center along the axial direction. Such a trend is compatible with the continuous heating along the pipe and

thus is physically sound.

The axial Nusselt number defined as $Nu(z^*) = \frac{1}{T_w^*(z^*) - T_b^*(z^*)}$ is plotted in figure 7. It shows a continuous decrease along the axial direction. Such a trend is explained by the fact that the temperature radial gradient is constant at the wall (constant heat flux); however, the difference between the wall temperature $T_w^*(z^*)$ and the mixing cup temperature $T_b^*(z^*)$ increases along the z^* direction . The difference is small at the entrance and increases continuously. It is established, Cebeci and Bradshaw [16], that for a sufficient length of the pipe, greater than what is called the thermal entry length, the temperature difference will level off and the axial $Nu(z^*)$ will reach its asymptotic value that is equal to 4.36. Our pipe length ($z^* = 100$) is slightly shorter that the thermal entry length ($z^* = 120$) and thus our axial $Nu(z^*)$ at $z^* = 100$ is slightly higher than 4.364 . It is equal to 4.793 which is the value published in the same reference for a length $z^* = 100$. The results of our reference state are found to be physically sound and numerically in excellent agreement with those of the specialized literature.

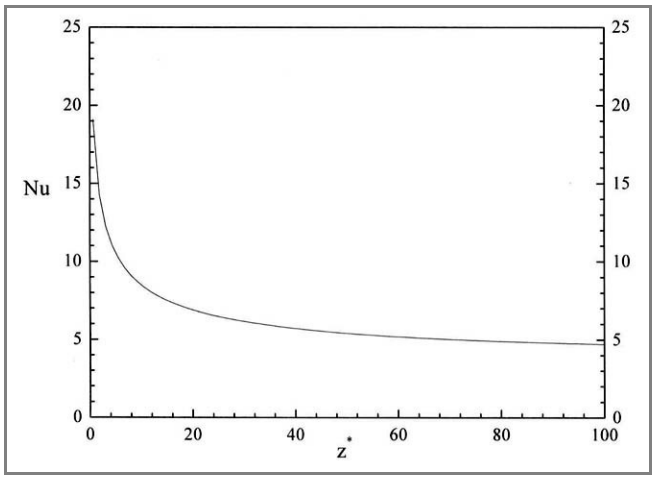

Figure 7: Axial Nusselt number for the reference state $Gr^*=0$.

3.2- The mixed convection case with $Gr^* = 10^6$

3.2.1- The flow field

This is a case with a Richardson number (Ri) equal to 1. The flow field of such a case cannot be axisymmetric. The only possible symmetry is that with respect to the vertical plane (parallel to the gravity vector) passing through the points θ=0 and θ=π. A transverse flow in the r^*-θ plane, at any z^* position, is possible as can be explained by the physics of induction of such a flow. Let us concentrate our attention on a single pipe section at a certain z^*. An imposed axisymmetric heat flux is imposed normal to the circumference of such a section. The imposed heat flux creates a radial temperature gradient: the temperature decreases radially from the circumference towards the section interior. The hot fluid is close to the perimeter while the relatively colder fluid is in the core of the section, surrounded by the hot fluid. At the upper part of the section the thermal stratification is stable as the hot, and thus lighter, fluid is above the colder core fluid. However, at the lower part of the section, the inverse case is present: the colder fluid is above the hot fluid which creates an unstable thermal stratification. A buoyant force is induced to overcome such instability, in the form of a convective circulation that tends to rise the hot fluid along the hot perimeter and lower the relatively cold fluid of the core towards the bottom of the section. The described convective motion must be symmetric with respect to the vertical plane passing through θ=0 and θ=π. Half the flow circulates counter clockwise in the right half section while the other half circulates clockwise in the left half section. This secondary flow was also obtained by the two-dimensional numerical simulations of Hong *et al.* [7] and Newell and Bergles [10].

The flow in the r^*-θ plane is affected by, but not induced by, the axial flow. The unstable thermal stratification in the lower part of the pipe is the only cause of induction of the flow in the r^*-θ plane. Thus for a uniformly heated horizontal pipe, the induction of a secondary transverse flow in the form of two counter-rotating vortices in the r^*-θ plane is physically sound and must be taken into account if a better modeling of the physics of the convective heat transfer is envisaged. This was done for the present case ($Gr^* = 10^6$) as illustrated by the model equations of the r^* and θ momenta. These contain $(Gr^*/\mathrm{Re}^2)T^*\cos\theta$ and $(Gr^*/\mathrm{Re}^2)T^*\sin\theta$ terms which properly model the buoyant forces along the r^* and θ directions, respectively. The transverse flow in the r^*-θ plane can be graphically visualized by the contours of the streamlines defined by : $V_\theta^* = -\frac{\partial \psi^*}{\partial r^*}$. This relation is integrated over selected sections at $z^* = 25$, 50, 75 and 100 and the contours plotting of the respective normalized streamlines are illustrated in figures 8a-8d. For better graphical representation, the stream function of each section is normalized by its maximum. The maxima are presented on the figures' captions. The previously discussed transverse flow is well present at all sections, in the form of the physically sound two counter-rotating vortices. Their circulation avoids the section top part (around θ =0) characterized by the stable thermal stratification. The vortices centers are closer to the pipe wall. As z^* increases from 25 to 50 the centers shift from the middle to the lower part of the section. Those of $z^* = 75$ and $z^* = 100$ are at the same position that is slightly lower than that of $z^* = 50$. Beyond $z^* = 75$, the secondary flow is quite hydrodynamically developed.

The transverse flow interacts with and affects the axial one. The latter one is expected to differ from that of the axisymmetric Poiseuille flow of the $Gr^* = 0$ case. The

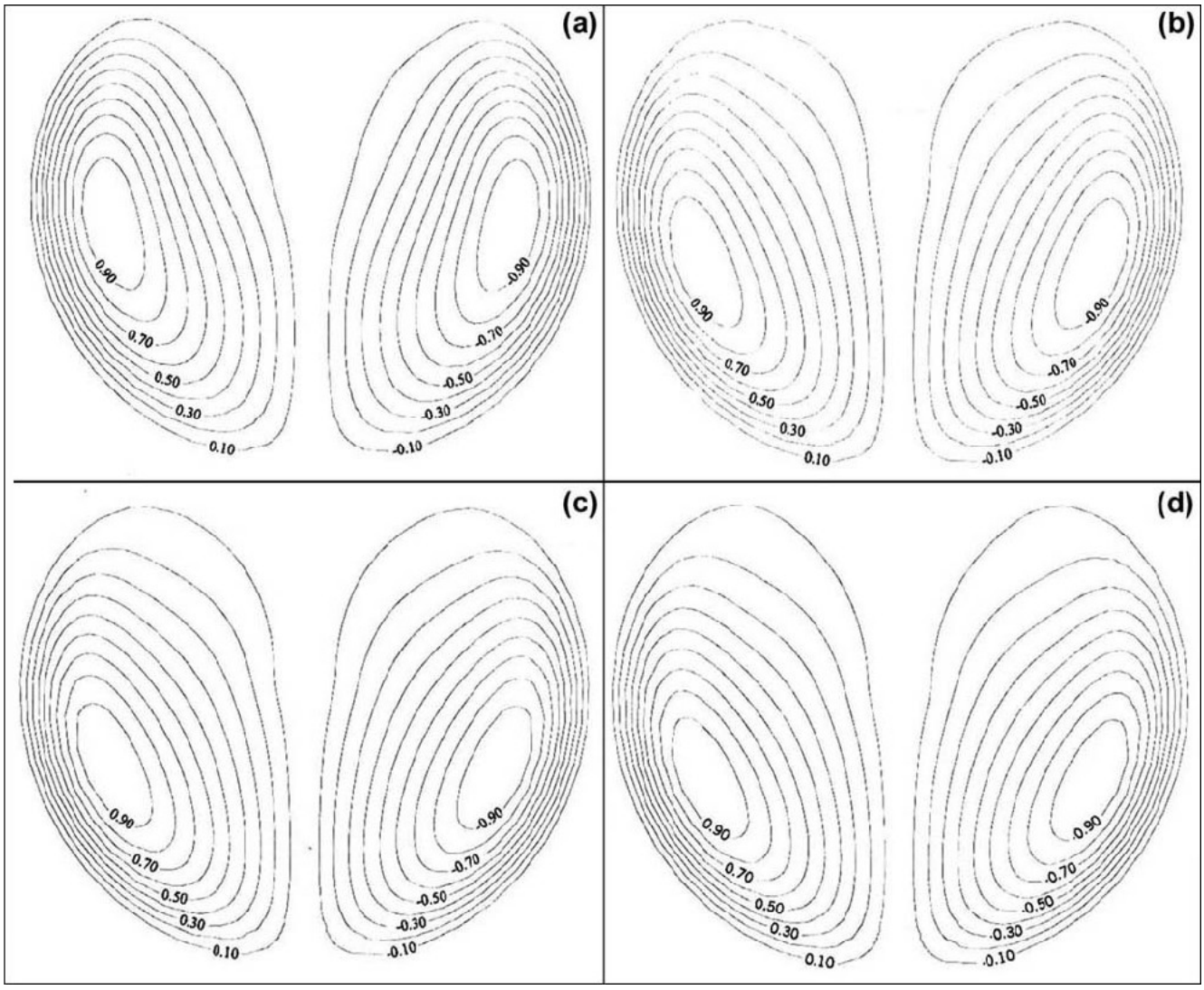

Figure 8: **(a)** Normalized streamlines ψ^* / ψ^*_{max} at z^*=25 for $Gr^*=10^6$ ($\psi^*_{max} = 0.00556$ at z^*=25).

(b) Normalized streamlines ψ^* / ψ^*_{max} at z^*=50 for $Gr^*=10^6$ ($\psi^*_{max} = 0.00395$ at z^*=50).

(c) Normalized streamlines ψ^* / ψ^*_{max} at z^*=75 for $Gr^*=10^6$ ($\psi^*_{max} = 0.00363$ at z^*=75).

(d) Normalized streamlines ψ^* / ψ^*_{max} at z^*=100 for $Gr^*=10^6$ ($\psi^*_{max} = 0.00357$ at z^*=100).

vortices of the secondary flow in the r^*-θ plane affect the transfer of the axial momentum. It is expected that the effect will be larger in the lower part of any section where the vortices motion is more important. This is the case as can be illustrated by the figures 9a-9d that represent the sectional variation of the axial velocity at the selected axial positions $z^* = 25,\ 50,\ 75$ and $z^* = 100$. The figures show that the distribution is not axisymmetric but symmetric with respect to the vertical line passing though $\theta = 0$ and $\theta = \pi$. This symmetry forces the location of the maximum velocity to be on this line. However, the maximum velocity is in the lower part of the line. The shifting of the velocity maximum to a position below the section center is due to the effect of the secondary flow that drives it downward. The combined motion, of the axial and the transverse flows, imparts to the fluid two helicoidal motions on the left and on the right of the vertical plane of symmetry. The helicoidal motion is the combination of the rotation in the r^*-θ plane and the translation in the axial direction. Since the rotation is mainly in the lower pipe region, the helicoidal motion is enhanced in this region causing the shifting of the maximum axial velocity towards the lower part of the pipe. It is noticed that the axial flow (and thus the whole flow) is quite hydrodynamically developed beyond $z^* = 75$.

3.2.2- The thermal field

The thermal field of the mixed convection flow is expected to be symmetric with respect to the vertical plane passing through θ=0 and θ=π, but cannot be axisymmetric. This is due to the rotational mixing caused by the secondary flow in the r^*-θ plane. Thus, at any pipe section, the heat

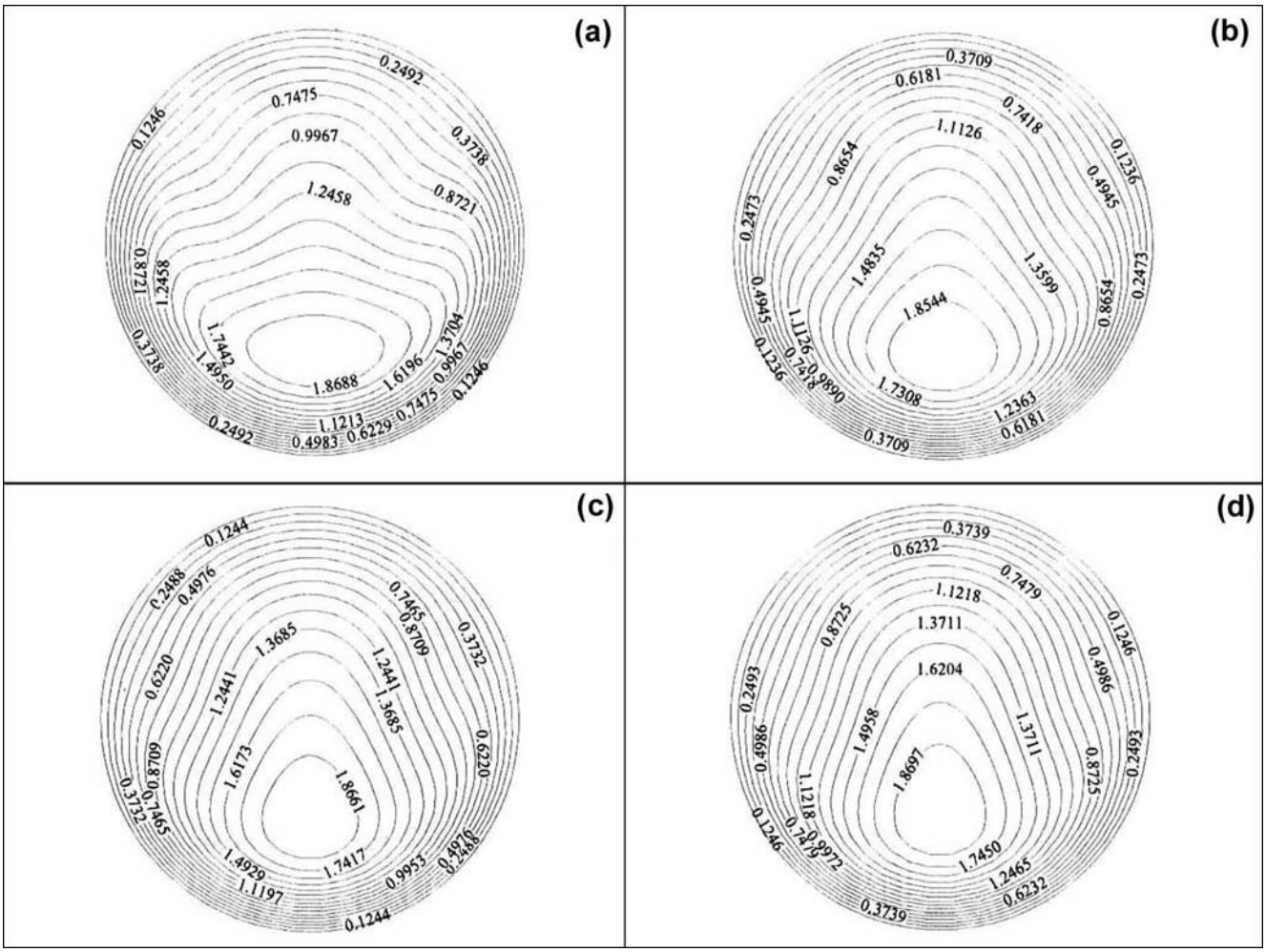

Figure 9: **(a)** Axial velocity contours at z^*=25 for $Gr^*=10^6$.
(b) Axial velocity contours at z^*=50 for $Gr^*=10^6$.
(c) Axial velocity contours at z^*=75 for $Gr^*=10^6$.
(d) Axial velocity contours at z^*=100 for $Gr^*=10^6$.

is diffused through the pipe wall and is convected along it. It is expected that the heat transfer will be enhanced in the lower portion of the pipe where an unstable thermal stratification is established and the rotating secondary flow is accelerated along the wall pipe. In the upper part of the section, the flow is hotter towards the wall. The maximum temperature must be on the plane of symmetry. Moreover, because of the imposed heat flux at the wall, the maximum sectional temperature must be at the wall. Thus, the maximum sectional temperature must be at the section top point (θ=0). The thermal stratification at the upper part of the section is stable. Moving radially inward from the wall to the section inner part, the temperature decreases towards the cold fluid core. This colder core is not centered around the pipe axis. It is in the lower section part. It is driven to this position by the rotational secondary flow. This is well illustrated by the figures 10a-10d showing the pipe sections thermal fields at $z^* = 25,\ 50,\ 75$ and 100, respectively. These sectional temperature profiles are qualitatively confirmed by the experiment of Pethukhov and Polyakov [5] who obtained exactly the same profiles for the case of (Ra = 2.8 10^7, Re = 960 and Pr =5). The thermal fields are normalized by the maximum non dimensional temperature ($T^* = 0.3771$) located at the top exit of the pipe. A comparison of such fields clearly reveals the increased axial heating of the fluid and the shifting of the cold core fluid towards the sections' lower parts under the effect of the better mixing due to the rotational flow in the r^*-θ plane. This better mixing will certainly lead to an enhancement of the heat transfer.

Figure 11 compares the axial variation of the mixing cup temperature and the wall temperature at three selected angular positions: $\theta = 0$, $\theta = \pi/2$ and $\theta = \pi$ corresponding to the top, the middle and the bottom parts of the section, respectively. It is noticed that all temperatures increase axially as expected. The mixing cup temperature rises linearly and the wall temperature decreases from θ=0 to θ=π, along the circumference. Up to the pipe exit, the mixing cup temperature remains lower than the minimum wall temperature (at θ=π).

In figure 12, we compare the axial local Nusselt number Nu(z^*) of the reference state ($Gr^* = 0$) and that of the $Gr^* = 10^6$ case. It is seen that the Nusselt number of the

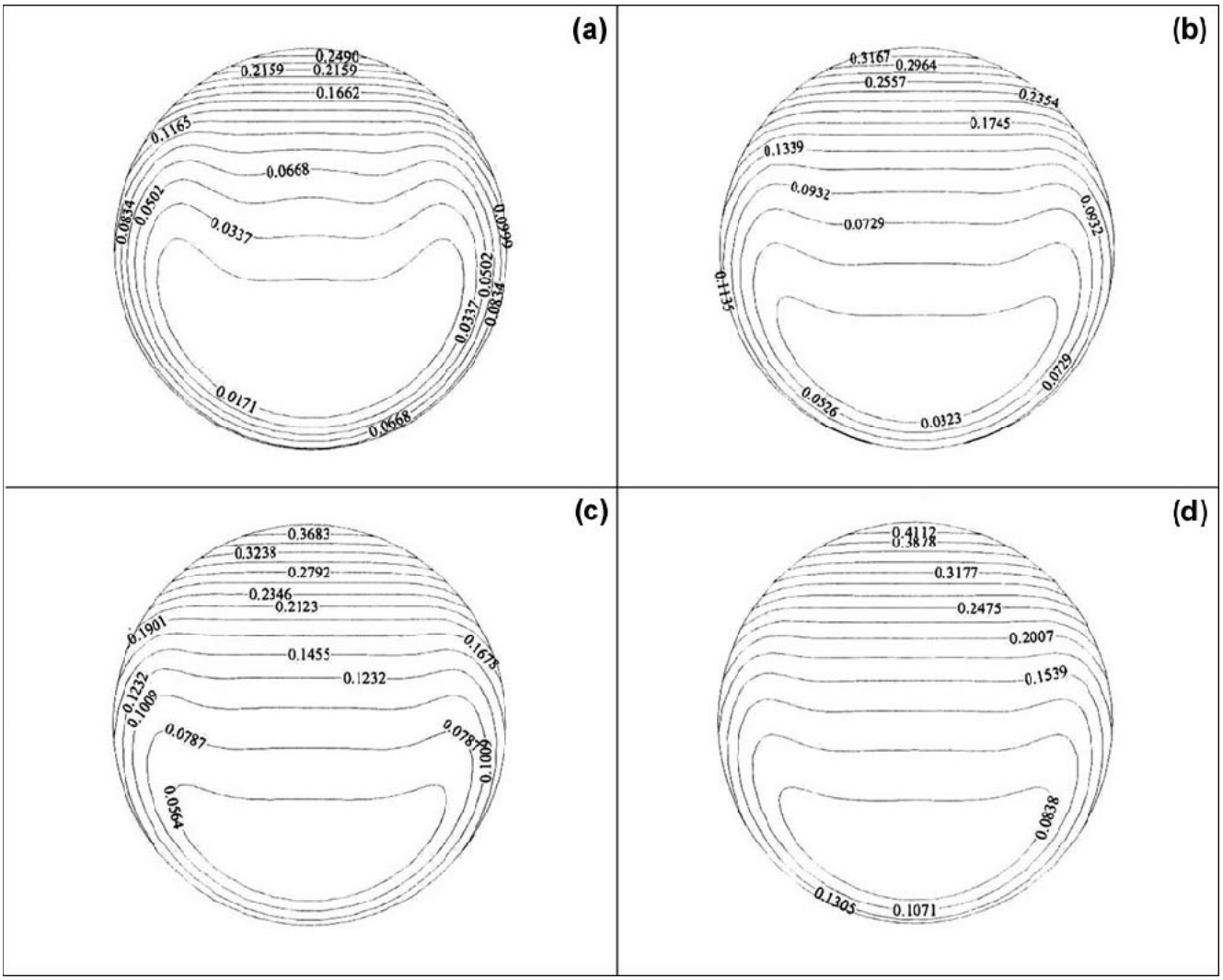

Figure 10: **(a)** Normalized isotherms $T^* / T^*_{\max}$ at z*=25 for Gr*=10^6 ($T^*_{\max} = 0.3771$ at the pipe exit).

(b) Normalized isotherms $T^* / T^*_{\max}$ at z*=50 for Gr*=10^6 ($T^*_{\max} = 0.3771$ at the pipe exit).

(c) Normalized isotherms $T^* / T^*_{\max}$ at z*=75 for Gr*=10^6 ($T^*_{\max} = 0.3771$ at the pipe exit).

(d) Normalized isotherms $T^* / T^*_{\max}$ at z*=100 for Gr*=10^6 ($T^*_{\max} = 0.3771$ at the pipe exit).

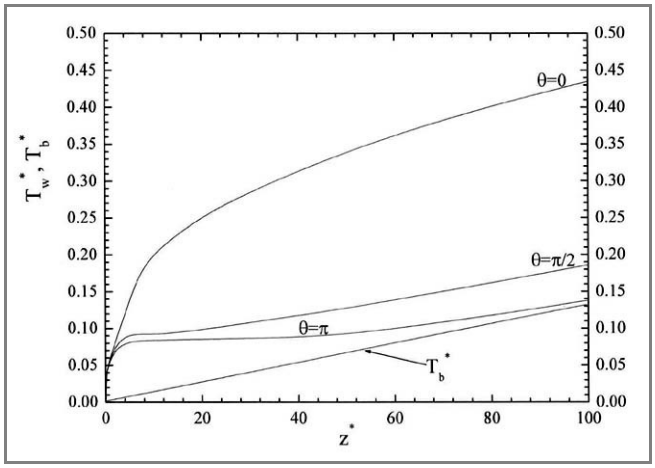

Figure 11: Axial variation of the bulk temperature T_b^* and the wall temperature T_w^* at $\theta = 0, \pi/2$ and π for Gr*=10^6.

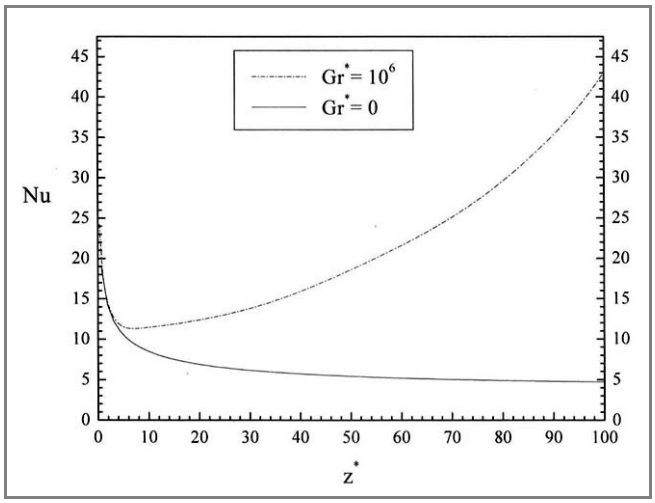

Figure 12: Variation of the local axial Nusselt numbers for Gr*=0 and 10^6.

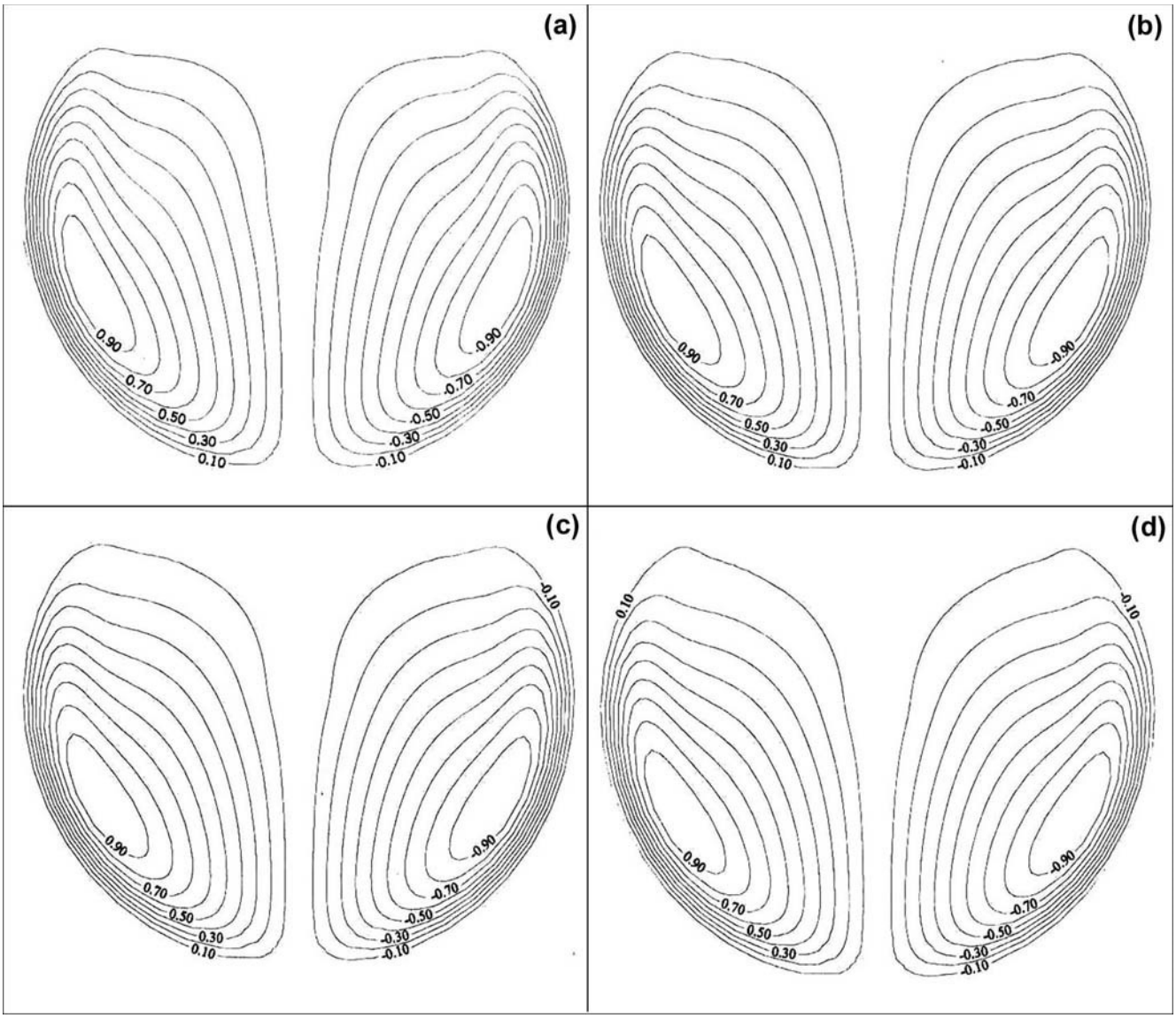

Figure 13: **(a)** Normalized streamlines ψ^* / ψ^*_{max} at z*=25 for Gr*=10^7 ($\psi^*_{max} = 0.00787$ at z*=25).

(b) Normalized streamlines ψ^* / ψ^*_{max} at z*=50 for Gr*=10^7 ($\psi^*_{max} = 0.00653$ at z*=50).

(c) Normalized streamlines ψ^* / ψ^*_{max} at z*=75 for Gr*=10^7 ($\psi^*_{max} = 0.00615$ at z*=75).

(d) Normalized streamlines ψ^* / ψ^*_{max} at z*=100 for Gr*=10^7 ($\psi^*_{max} = 0.00617$ at z*=100).

reference state decreases continuously along the axial direction whereas that of $Gr^* = 10^6$ decreases from the entrance of the pipe to a distance around $z^* = 8$ and then increases continuously from that position to the exit. Such an increase characterizes the enhancement of the heat transfer due to the mixing imparted to the fluid by the rotational flow. The qualitative axial increase of the local Nusselt number was also reported by an experimental mixed convection study by Shannon and Depew [2].

3.3- The mixed convection case with Gr* = 10^7

3.3.1- The flow field

The flow field of such case corresponds to a Richardson number (Ri =10). This flow field is expected to be qualitatively similar to that of $Gr^* = 10^6$ but with a more intensive rotational flow. The buoyant force is larger and the fluid mixing is enhanced. The rotational flow is presented in figures 13a-13d. As in the case of $Gr^* = 10^6$, at all sections, two counter-rotating vortices are observed but they are stronger as proven by the increased values of the stream function at any section (see the maxima of the stream function presented on figures' captions). This increased strength of the rotational flow is expected to have an increased effect on the axial flow profile and on the local heat transfer. Moreover, it is noticed that beyond $z^* = 75$, the rotational flow is hydrodynamically quite developed along the axial direction.

The axial velocity profiles shown in figures 14a-14d are qualitatively similar to those of the $Gr^* = 10^6$ case but have

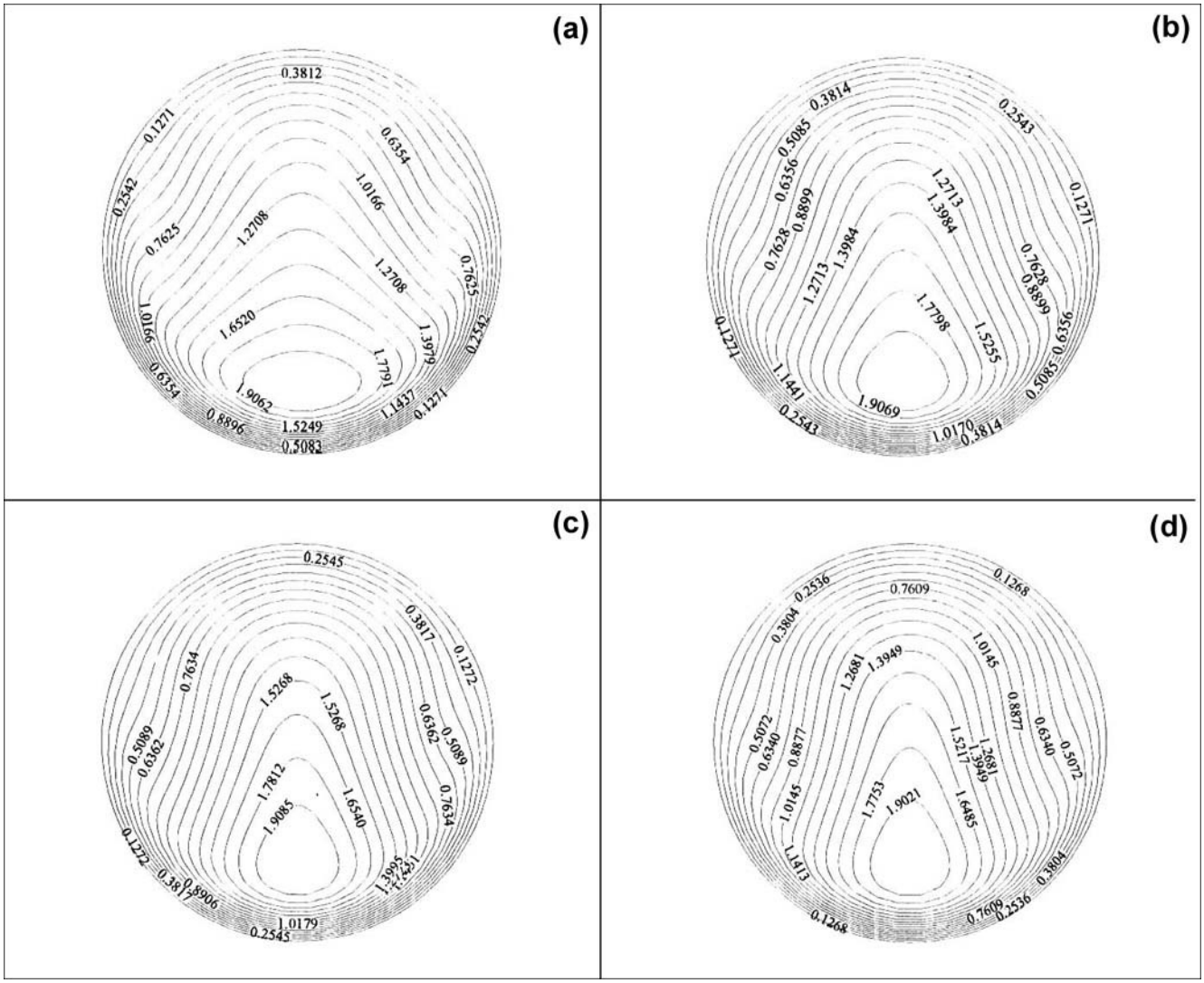

Figure 14: **(a)** Axial velocity contours at z^*=25 for $Gr^*=10^7$.
(b) Axial velocity contours at z^*=50 for $Gr^*=10^7$.
(c) Axial velocity contours at z^*=75 for $Gr^*=10^7$.
(d) Axial velocity contours at z^*=100 for $Gr^*=10^7$.

larger angular variations. The higher velocity shifts towards the lower part of the sections and larger radial velocity gradients are observed between the position of the maximum velocity and the bottom of the sections. Of course these larger variations are due to the enhancement of the rotational flow.

3.3.2- The thermal field

The thermal field at the same four axial stations $z^* = 25, 50,$ 75 and 100 are presented in figures 15a-15d. The axial increase of the temperature is very clear. The field is normalized by the maximum non dimensional temperature $T^* = 0.3318$ at the top exit of the pipe. Away from the wall, a stable thermal stratification is observed from the section top down to the cold fluid core at the bottom of the section. However, from the cold core to the bottom point the temperature increases and the thermal stratification in unstable.

An interesting physical phenomenon is encountered for this case (with Ri = 10). It is the reaching of the mixing cup temperature its upper possible limit which is the wall temperature at the bottom of the pipe. This is illustrated in figure 16 where the axial variation of the wall temperature at $\theta = 0$, $\theta = \pi/2$ and $\theta = \pi$ is compared with that of the mixing cup temperature. The mixing cup temperature remains lower than the wall temperature at $T^* = 0.3318$; however, it asymptotically approaches the wall temperature at $\theta = \pi$ at some axial location near $z^* = 70$. We attempt a physical explanation of such a phenomenon. We first note that the mixing cup temperature (as defined) increases linearly in the axial direction due to the constant wall heat flux. Moreover, the increase of the wall temperature at $\theta = \pi$ gets lower downstream (compared to that of θ=0) because of the motion of the cold fluid core towards the bottom part of the pipe under the effect of the secondary flow. Furthermore, the mixing cup temperature cannot be

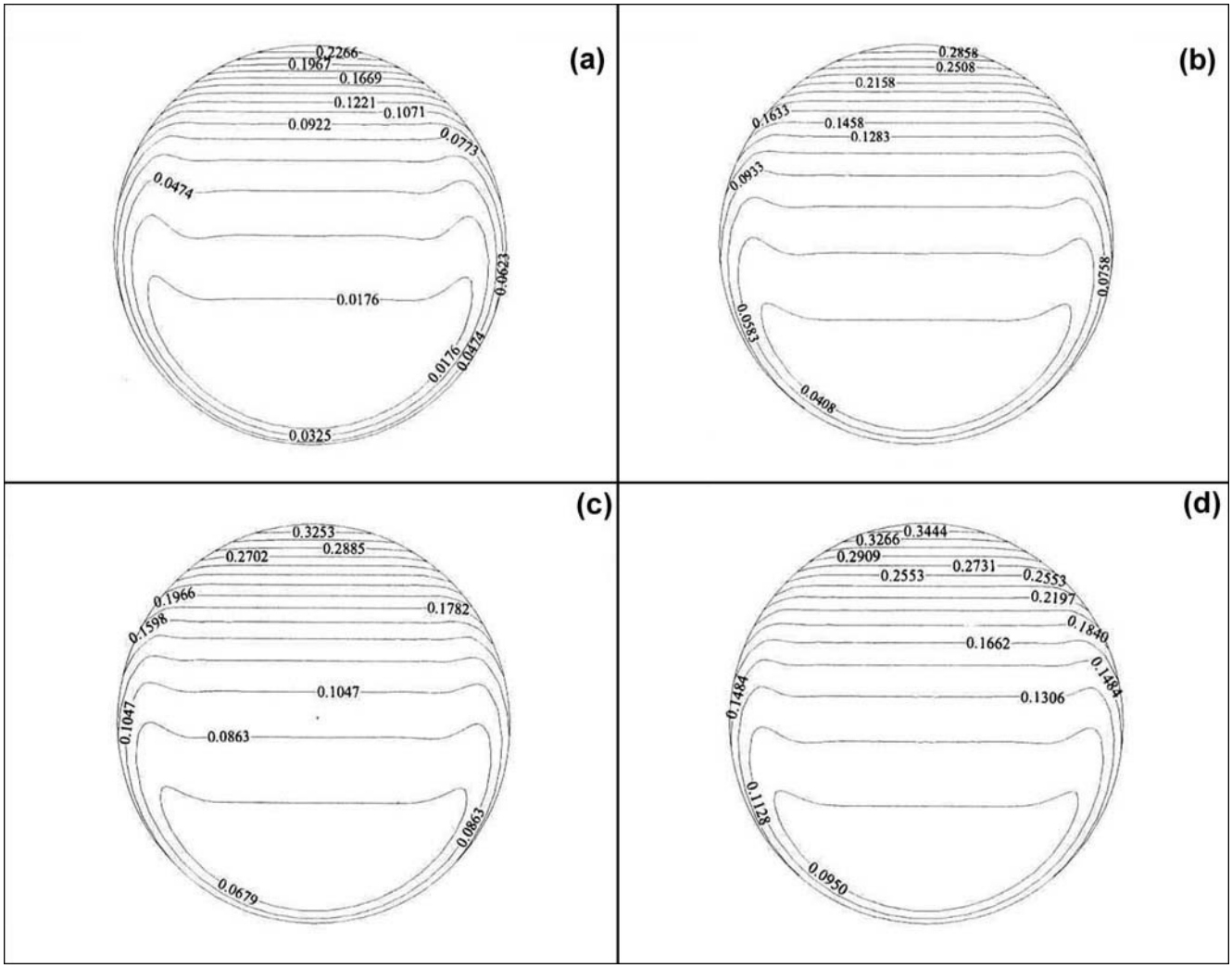

Figure 15: **(a)** Normalized isotherms $T^* / T^*_{\max}$ at z*=25 for Gr*=10^7 ($T^*_{\max} = 0.3318$ at the pipe exit).

(b) Normalized isotherms $T^* / T^*_{\max}$ at z*=50 for Gr*=10^7 ($T^*_{\max} = 0.3318$ at the pipe exit).

(c) Normalized isotherms $T^* / T^*_{\max}$ at z*=75 for Gr*=10^7 ($T^*_{\max} = 0.3318$ at the pipe exit).

(d) Normalized isotherms $T^* / T^*_{\max}$ at z*=100 for Gr*=10^7 ($T^*_{\max} = 0.3318$ at the pipe exit).

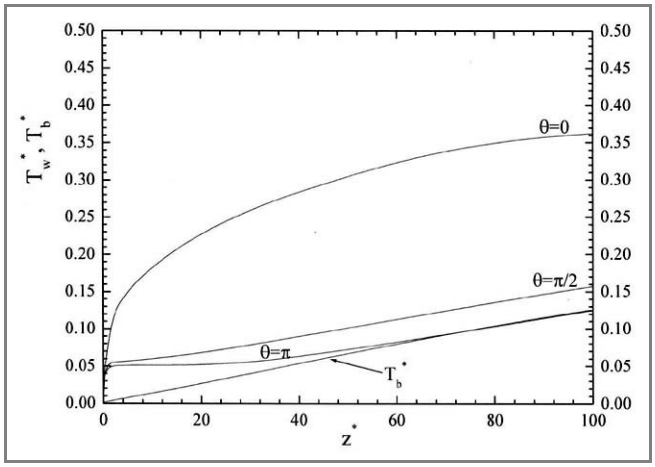

Figure 16: Axial variation of the bulk temperature T^*_b and the wall temperature T^*_w at $\theta = 0$, $\pi / 2$ and π for Gr*=10^7.

higher than any wall temperature because of the imposed thermal boundary condition: a heat flux from the wall to the fluid. This makes the minimum wall temperature (at the bottom of the pipe) an upper bound for the mixing cup temperature. A bound that the mixing cup temperature approaches asymptotically beyond $z^* = 70$. Beyond this z^*, the bottom wall temperature may be considered a measure of the mixing cup temperature. This makes the local Nusselt number defined as $\dfrac{1}{T^*(1/2,\, \theta,\, z^*) - T^*_b(z^*)}$ infinite at the bottom of the wall (where $\theta = \pi$ and $T^*_b(z^*) \to T^*(1/2,\, \theta, z^*)$). The local axial Nusselt number $Nu(z^*)$, as defined, also goes to infinity beyond $z^* = 70$.

The axial Nusselt numbers of $Gr^* = 0$, $Gr^* = 10^6$ and $Gr^* = 10^7$ are compared in figure 17. There, it is seen that

the enhancement of heat transfer due to the mixing caused by the secondary flow is much more important for the $Gr^* = 10^7$ case. Such a case cannot be simulated by a forced convection model.

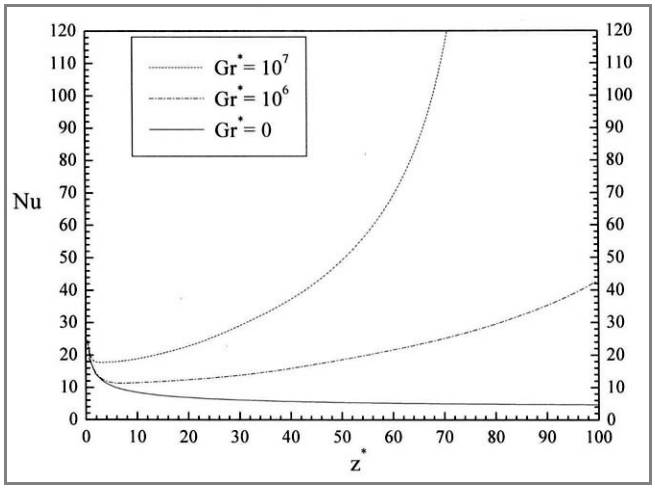

Figure 17: Comparison of the local axial Nusselt numbers of the three Grashof numbers: 0, 10^6, 10^7.

CONCLUSION

The three-dimensional convection in a uniformly heated horizontal pipe is considered. The pipe has an aspect ratio equal to 100 and transports a fluid with a constant Prandtl number $Pr = 3.02$ at a constant Reynolds number $Re = 1000$. Three Grashof numbers are considered: $Gr^* = 0$ corresponding to a forced convection and $Gr^* = 10^6$ and $Gr^* = 10^7$ corresponding to the increased effect of mixed convection. A finite volume numerical method with a uniform grid 43x44x165 points is used to solve the model equations by a time marching scheme. The flow field of the mixed convection cases are not axisymmetric and differ significantly from that of the reference state. The induction of the flow in the r^*-θ plane makes these flows three-dimensional. These flows impart to the fluid a helicoidal motion that enhances its mixing downstream. This mixing enhances the heat transfer significantly. It is remarkable that for the $Gr^* = 10^7$ case, the mixing effect raises the mixing cup temperature to its allowable upper bound (the minimum wall temperature).

Nomenclature

A : aspect ratio = L/D
D : pipe diameter (m)
g : gravitational acceleration (m·s^{-2})
Gr^* : modified Grashof number = $(g\beta/\nu^2)\,(q_w D/k)\,D^3$
$h(\theta,z^*)$: local heat transfer coefficient (W·m^{-2}·K^{-1})
k : fluid thermal conductivity (W·m^{-1}·K^{-1})
L : pipe length (m)
$Nu(\theta,z^*)$: local Nusselt number
$Nu(z^*)$: circumferentially averaged local axial Nusselt number
Pr : Prandtl number = ν/α
P : pressure (N·m^{-2})
P^* : non dimensional pressure = $(P - P_0)/\rho_0 V_0^2$
q_w : pipe wall heat flux (W·m^{-2})
R : pipe radius (m)
Re : Reynolds number = $V_0 D/\nu$
Ri : Richardson number = Gr^*/Re^2
R : radial coordinate (m)
r^* : non dimensional radial coordinate = r/D
t : time (s)
t^* : non dimensional time = $t(V_0/D)$
T : temperature (K)
T^* : non dimensional temperature = $(T - T_0)/(q_w D/k)$
T_b : mixing section temperature (K)
T_b^* : non dimensional mixing temperature = $(T_b - T_0)/(q_w D/k)$
V_0 : mean axial velocity at the entrance (m·s^{-1})
V_r : radial velocity component (m·s^{-1})
V_r^* : non dimensional radial velocity component = V_r/V_0
V_θ : circumferential velocity component (m·s^{-1})
V_θ^* : non dimensional circumferential velocity component = V_θ/V_0
V_z : axial velocity component (m·s^{-1})
V_z^* : non dimensional axial velocity component = V_z/V_0
Z : axial coordinate (m)
z^* : non dimensional axial coordinate = z/D

Greek symbols

α : thermal diffusivity (m²·s^{-1})
β : thermal expansion coefficient (K^{-1})
θ : angular coordinate (rad)
ν : kinematic viscosity (m²·s^{-1})
ρ : density (kg·m^{-3})
ψ^* : non dimensional stream function

Subscripts

w : reference to the pipe wall
0 : reference to the pipe entrance

Superscript

* : reference to non dimensional

Acknowledgments

• A 3-D Fortran code for general numerical solutions of heat transfer and fluid mechanics in cylindrical coordinates was provided by Dr. A. Zebib of the Mechanical and Aerospace Engineering Department of Rutgers University, New-Jersey, U.S.A.

•This study was financially supported by the Algerian M.E.S.R.S. through the grant of the project identified as D2501/04/97.

•The bibliographic support was provided by F. Papini and C. Abid , I.U.S.T.I., CNRS UMR 139, Université de Provence, Technopôle Château Gombert, Marseille, France.

REFERENCES

[1]- Mori Y., Futagami K., Tokuda S., "Nakamura N., Forced convective heat transfer in uniformly heated horizontal tube", 1st report experimental study on the effect of buoyancy, *Int. J. Heat Mass Transfer*, Vol.9, (1966), pp. 453-463.

[2]- Shannon R.L., Depew C.A., "Combined free and forced laminar convection in a horizontal tube with uniform heat flux", *ASME J. Heat Transfer*, Vol.90, (1968), pp.353-357.

[3]- Shannon R.L., Depew C.A., "Forced laminar flow convection in a horizontal tubes with variable viscosity and free convection effects", *ASME J. Heat Transfer*, Vol. 91, (1969), pp. 251-258.

[4]- Hussaïn N.A., McComas S.T., "Experimental Investigation of combined convection in a horizontal circular tube with uniform heat flux", Proceedings of the Fourth Int. Heat Transfer Conf., Elseiver, Amsterdam, Vol. 4 (1970), NC 3.4.

[5]- Pethukhov B.S., Polyakov A.F., "Flow and heat transfer in horizontal tubes under combined effect of forced and free convection", Proceedings of the Fourth Int. Heat Transfer Conf., Elsevier, Amsterdam, Vol. 4 (1970), NC 3.7.

[6]- Bergles A.E., Simonds R.R., "Combined forced and free convection for laminar flow in horizontal tubes with uniform heat flux", *Int. J. Heat Mass Transfer*, Vol. 14, (1971), pp. 1989-2000.

[7]- Hong S.W., Morcos S.M., Bergles A.E., "Analytical and experimental results for combined forced and free laminar convection in horizontal tubes", Proc. of the Fifth Int. Heat Transfer Conf., Tokyo, Vol. 3 (1974), pp. 154-158.

[8]- Morcos S.M., Bergles A.E., "Experimental investigation of combined forced and free laminar convection in horizontal tubes", *ASME J. Heat Transfer*, Vol.97, (1975), pp. 212-219.

[9]- Abid C., Papini F., Ropke A., Veyret D., "Etude de la convection mixte dans un conduit cylindrique. Approche analytique / numérique et détermination expérimentale de la température de paroi par thermographie infrarouge", *Int. J. Heat Mass Transfer*, Vol.37, (1994), pp. 91-101.

[10]- Newell Jr. P.H., Bergles A.E., "Analysis of combined free and forced convection for fully developed laminar flow in horizontal tubes", *ASME J. Heat Transfer*, Vol.92, (1970), pp. 83-93.

[11]- Patankar S.V., Ramadhyani E., Sparrow E.M., "Effect of circumferentially non uniform heating on laminar combined convection in a horizontal tube", *ASME J. Heat Transfer*, Vol.100, (1978), pp. 63-70.

[12]- Law H.S., Masliyah J.H., Nandakumar V., "Effect of non uniform heating on laminar mixed convection in ducts", *ASME J. Heat Transfer*, Vol.109, (1987) pp.131-137.

[13]- Ouzzane M. et Galanis N., "Effets de la conduction pariétale et de la répartition du flux thermique sur la convection mixte près de l'entrée d'une conduite inclinée", *Int. J. Thermal Sciences*, Vol.38, (1999), pp. 622-633.

[14]- Patankar S.V., "Numerical Heat Transfer and Fluid Flow", Mc Graw Hill, New-York, (1980).

[15]- Polyakov A.F., "Mixed Convection in Single-Phase Flows", in O.G. Martynenko and A. A. Zukauskas (eds.), Heat Transfer: Soviet Reviews, Convective Heat Transfer,Vol.1, Hemisphere, Washington, D.C, (1989) pp.1-95.

[16]- Cebeci T., Bradshaw P., "Physical and Computational Aspects of Convective Heat Transfer", Springer-Verlag, New-York, (1984). □